Flow Structures With High Lagrangian Coherence Rate Promote Diatom Blooms in Oligotrophic Waters

Ismael Hernández-Carrasco, Vincent Rossi, Gabriel Navarro, Antonio Turiel, Annalisa Bracco, Alejandro Orfila

Geophysical Research Letters

RESEARCH LETTER
10.1029/2023GL103688

Flow Structures With High Lagrangian Coherence Rate Promote Diatom Blooms in Oligotrophic Waters

Ismael Hernández-Carrasco[1], Vincent Rossi[2], Gabriel Navarro[3], Antonio Turiel[4], Annalisa Bracco[5], and Alejandro Orfila[1]

[1]Mediterranean Institute for Advanced Studies (UIB-CSIC), Esporles, Spain, [2]Mediterranean Institute of Oceanography, CNRS, UMR, Marseille, France, [3]ICMAN (CSIC), Cadiz, Spain, [4]ICM (CSIC), Passeig Marítim de la Barceloneta, Barcelona, Spain, [5]School of Earth and Atmospheric Sciences, Georgia Institute of Technology, Atlanta, GA, USA

Key Points:

- Combined Lagrangian assessments of flow kinematic properties to analyze the range of dynamical coherence scales in geophysical flows
- Lagrangian coherence rate is a new metric to identify dynamically-relevant flow structures
- Observations evidence that highly-coherent flow structures in high vorticity and kinetic energy promote diatom blooms in oligotrophic waters

Supporting Information:

Supporting Information may be found in the online version of this article.

Correspondence to:

I. Hernández-Carrasco, ihernandez@imedea.uib-csic.es

Citation:

Hernández-Carrasco, I., Rossi, V., Navarro, G., Turiel, A., Bracco, A., & Orfila, A. (2023). Flow structures with high Lagrangian coherence rate promote diatom blooms in oligotrophic waters. *Geophysical Research Letters*, *50*, e2023GL103688. https://doi.org/10.1029/2023GL103688

Received 16 MAR 2023
Accepted 26 JUL 2023
Corrected 23 AUG 2023

This article was corrected on 23 AUG 2023. See the end of the full text for details.

Author Contributions:

Conceptualization: Ismael Hernández-Carrasco, Vincent Rossi, Alejandro Orfila
Data curation: Gabriel Navarro
Formal analysis: Ismael Hernández-Carrasco, Antonio Turiel, Annalisa Bracco, Alejandro Orfila
Funding acquisition: Alejandro Orfila

Abstract Diatoms are among the most efficient autotrophic organisms for oceanic primary production and carbon sequestration. Yet, the spatial distributions of these planktonic organisms remain puzzling and the underlying physical processes poorly known, especially in oligotrophic open waters. Here we investigate what dynamical conditions are conducive to episodic diatom blooms in oceanic deserts based on Lagrangian diagnosis and satellite-derived phytoplankton functional types and currents. The coherence of the flow is diagnosed in space and time simultaneously through the Lagrangian coherence rate (LCR) to identify which dynamical structures favor diatom growth. Observations evidence that flow structures with high LCR (40 days or longer) in areas with elevated eddy kinetic energy and vorticity sustain high diatom concentrations in the sunlit layers. Our findings show that the integration of Eulerian kinematic variables into a Lagrangian frame reveals new dynamical aspects of geophysical turbulence and unveil their biological impacts.

Plain Language Summary Marine diatoms are amongst the largest photosynthetic plankton that play an important role in the oxygen cycling and the removal of carbon dioxide from the atmosphere. However, their abundance is predicted to decline as a result of the increasing ocean stratification induced by global warming. Understanding the underlying physical processes that are conducive to diatom blooms is crucial to accurately predict the evolution of primary production and carbon export. Here using a novel measure of the range of dynamical coherence scales applied to satellite observations, we provide evidences that flow structures surpassing a quantitative threshold of coherence in high mesoscale activity and vorticity provide the favorable dynamical conditions sustaining diatoms growth in stratified and oligotrophic waters.

1. Introduction

Earth System model simulations as well as mesocosm experiments indicate that in response to increased ocean stratification and reduced vertical mixing caused by global warming, diatoms are likely to decline or be replaced by smaller phytoplankton (Barton et al., 2016; Frémont et al., 2022). However, these model predictions do not account for the role of the physical environment at scales smaller than 100 km in structuring the distribution of phytoplankton functional types. Understanding the role played by the ocean circulation at these scales in the development of diatoms in stratified and oligotrophic waters is essential to accurately predict the future evolution of primary production and carbon export (Falkowski et al., 1998; Field et al., 1998; Tréguer et al., 2018).

In contrast to other groups of smaller plankton, such as dinoflagellates, which are favored under stratified, low-nutrient conditions, diatoms are known to thrive in high nutrient systems (e.g., polar, upwelling and coastal areas). They are, however, not exclusive to these systems, and recent observations revealed that short-living spatially-restricted diatoms blooms may occur in oligotrophic, nutrient limited waters (Malviya et al., 2016). These blooms are fueled by transient meso- and submesoscale dynamical turbulent structures such as eddies, fronts or filaments (Hernández-Carrasco et al., 2020; Tréguer et al., 2018), that modulates the mixed layer depth (Gaube et al., 2019), and thus, temporally bring nutrients into the euphotic zone. While these turbulent structures are often characterized by vertical velocities on scales small enough to have ageostrophic contributions—which are hard to detect and measure—, they also have an imprinting on the mesoscale flow (Liu et al., 2021). This imprinting is the focus of our investigation. Because of the small scale ageostrophic contributions, it is not yet possible to link specific dynamical structures to functional phytoplankton groups. On one hand, model-based studies are strongly dependent on the modeling formulation and how the interactions between biological and

Investigation: Ismael Hernández-Carrasco, Vincent Rossi, Annalisa Bracco, Alejandro Orfila
Methodology: Ismael Hernández-Carrasco, Vincent Rossi
Software: Ismael Hernández-Carrasco
Visualization: Ismael Hernández-Carrasco
Writing – original draft: Ismael Hernández-Carrasco
Writing – review & editing: Ismael Hernández-Carrasco, Vincent Rossi, Gabriel Navarro, Antonio Turiel, Annalisa Bracco, Alejandro Orfila

physical processes are parameterized (Barton et al., 2010; D. J. McGillicuddy, 2016). On the other hand, observational studies remain scarce due to the lack of simultaneous measurements of velocity fields and phytoplankton taxonomy at large scale (Hernández-Carrasco et al., 2020). Furthermore, most monitoring studies occur at a fixed location, linking the characteristics of the local phytoplankton communities to some properties of the Eulerian ("frozen" in space) flow (Cotti-Rausch et al., 2016). Contrasting with the Eulerian view, an important issue when studying bio-physical interactions in fluid environments is that any physically-driven phytoplankton community shift or change in activity (Lévy et al., 2014; Wilkins et al., 2013) would reflect the cumulative effects of coherent transport dynamics affecting nutrient supply and other growth-limiting factors.

In this study we propose a methodology to classify the flow structures according to their Lagrangian coherence rates. The method is based on the Lagrangian assessment F of an Eulerian kinematic variable f, which provides information on the cumulative effect of f along trajectories, as it integrates the observed variable over the time-evolution of moving water parcels arriving to a specific point. The finite-time dynamical systems theory has shown that relevant information regarding the dynamical properties of the flow can be inferred from F, especially when f is chosen to be a function related to the velocity field (Haller & Poje, 1998; Mezić et al., 2010). Here we chose to assess coherent transport processes through the finite-time Lagrangian integration of vorticity and eddy kinetic energy (EKE), denoted by Ω_T and K_T, respectively. This methodology allows for investigating the impact of Lagrangian persistent lateral turbulent properties of the underlying flow structures on the phytoplankton community structure. In particular, the combination of Ω_T and K_T allows to accurately assess the spatial and temporal coherence rates (i.e., LCR) of turbulent structures that do or do not favor a sustained growth of diatoms, providing a robust diagnostic to identify, among all the eddies, those associated with a biological response. Previously developed Lagrangian flow diagnostics, such as Lyapunov exponents based Lagrangian coherent structures (Hernández-Carrasco et al., 2011) have shown to be very useful to identify dynamical boundaries separating different functional phytoplankton groups (d'Ovidio et al., 2010). The proposed methodology allows to identify not only the boundaries but also to quantify the characteristic dynamical scales of the underlying flow associated with a particular functional phytoplankton group.

We apply this framework to data from two independent sources of satellite observations. Specifically, we use data of dominant phytoplankton functional type (PFT) from a regional adaptation of the PHYSAT algorithm (Navarro et al., 2017) and daily velocity fields at 1/8° of spatial resolution derived from a Ssalto/Duacs multimission altimeter regional product. We focus on the Mediterranean Sea, which is characterized by intense mesoscale activity (d'Ovidio et al., 2009; Morales-Márquez et al., 2023) and by high productivity only during spring time, between February and April (Basterretxea et al., 2018), with dominance of large phytoplanktonic cells such as diatoms (Navarro et al., 2017). During the rest of the year is on average oligotrophic and highly stratified, disrupted by local—in time and space—events of elevated phytoplankton growth. The Mediterranean Sea is therefore a good proxy for ocean deserts, which cover most of the global ocean, offering an ideal laboratory to explore the biological response of an oligotrophic and highly stratified environment to intermittent, dynamical changes in the physical structure of the upper ocean.

2. Finite-Time Lagrangian Diagnostics

Given an Eulerian descriptor f, its Lagrangian counterpart F can be obtained by computing the path-integral of f. It can be expressed in a general way by the material integration of f along the fluid parcel trajectory, $\mathbf{R}_T(\mathbf{r}_0, t_0)$, initially located at $\mathbf{r}_0(t_0)$ over a finite time interval of integration T as, $F_T(\mathbf{r}_0, t_0) = \frac{1}{T}\int_{t_0}^{t_0+T} f(\mathbf{R}_t(\mathbf{r}, t_0), t)dt$. The ergodic theory of dynamical systems asserts that when $T \to \infty$ such Lagrangian functions should be constant along invariant manifolds, independently of the Eulerian function chosen. This property has been used to extract the flow geometry in autonomous or periodic dynamical systems (Haller & Poje, 1998). Nevertheless the ocean flow is dynamically an aperiodic and finite system; consequently this kind of functions can only be path-integrated (or averaged in a Lagrangian sense) over a finite time period ($T \ll \infty$). Even so, relevant information regarding the dynamical properties of the flow can still be inferred from F, especially when f is chosen to be related to the velocity field, $\mathbf{v}$ (Haller & Poje, 1998; Mezić et al., 2010). Here we quantify transport coherent processes extending the choice of f to relative vorticity (ω) and EKE, since EKE informs on the turbulent component of the flow associated with eddy activity, while ω takes into account the shear and the rotation of the flow.

Considering the motion of a fluid parcel on the time interval $[t_0, t_0 + T]$, we define the finite-time Lagrangian vorticity (FTLV), denoted by Ω_T, at the position $\mathbf{r}_0 = (x_0, y_0)$ at time t_0 based on the objective (i.e., invariant with

respect to Euclidean frame changes) definition of relative dynamic rotation angle for two-dimensional flows reported in Haller (2016), as:

$$\Omega_T(\mathbf{r}_0, t_0, T) = \int_{t_0}^{t_0+T} (\omega(\mathbf{R}_t(\mathbf{r}, t_0), t) - \langle\omega(t)\rangle)\, dt, \tag{1}$$

where ω is the z-component of the vorticity vector: $\omega(\mathbf{r}, t) = \frac{\partial v(\mathbf{r},t)}{\partial x} - \frac{\partial u(\mathbf{r},t)}{\partial y}$ and $\langle\omega\rangle$ its spatial average, which is averaged over a domain to be chosen large enough so that the averaged vorticity is representative of the overall mean rotation of the flow under study. For geostrophic flows, the mean rotation is expected to be zero, which has been confirmed for the Mediterranean Sea (not shown), and Ω_T takes the form:

$$\Omega_T(\mathbf{r}_0, t_0, T) = \frac{1}{T}\int_{t_0}^{t_0+T} \omega(\mathbf{R}_t(\mathbf{r}, t_0), t)\, dt, \tag{2}$$

The Lagrangian description of the vorticity was also used to develop an objective identification of coherent vortex boundaries based on well-defined contours of Lagrangian-averaged vorticity deviation (LAVD) (Haller et al., 2016). While LADV provides a measure of the intrinsic dynamical rotation (Haller, 2016) (which is always positive) the FTLV also allows the quantification of the net rotation angle, accounting for changes in the sign of the rotation.

Furthermore, we use a complementary metric to analyze the evolution of the EKE along fluid parcel trajectories. Specifically, we compute the finite-time Lagrangian EKE (FTLK), denoted by K_T, as follows:

$$K_T(\mathbf{r}_0, t_0, T) = \frac{1}{T}\int_{t_0}^{t_0+T} \kappa(\mathbf{R}_t(\mathbf{r}, t_0), t)dt, \tag{3}$$

where κ is the Eulerian EKE given by, $\kappa(\mathbf{r}, t) = \left(u(\mathbf{r}, t) - \langle u(\mathbf{r})\rangle_{\Delta T}\right)^2 + \left(v(\mathbf{r}, t) - \langle v(\mathbf{r})\rangle_{\Delta T}\right)^2$, obtained through the instantaneous anomaly of the zonal and meridional components of the velocity field with respect to the steady mean of the total kinetic energy, which is achieved averaging over a time period $\Delta T = 10$ years. High values of K_T identify therefore regions where the flow is concentrating mesoscale activity. The LCR is, therefore, obtained from the time integration T associated with a Lagrangian-persistent value of K_T and Ω_T. These diagnostics allow classifying the flow, in the domain under consideration, in subregions according to the LCR values.

3. Satellite Data

The identification from satellite observations of the dominant phytoplankton functional type (PFT), is performed using the PHYSAT algorithm (Alvain et al., 2005). Here we use a regional adaptation of this algorithm to the specific bio-optical characteristics of the Mediterranean Sea, PHYSAT-Med (Navarro et al., 2014, 2017). The PHYSAT-Med identifies nanoeukaryotes, coccolithophorids, *Prochlorococcus*, *Synechococcus*-like cyanobacteria, diatoms and Phaeocystis-like phytoplankton through the analysis of the specific signatures in the normalized water-leaving radiance (nLw) spectra measured by ocean color sensors. For this study, we use the PHYSAT-Med version published in 2017 (Navarro et al., 2017), in which the authors used the OC-CCI v3.0 data set generated from merged normalized remote-sensing reflectance derived from four satellite sensors (Storm et al., 2013): SeaWiFS, MODIS, MERIS, and VIIRS. PHYSAT-Med retrieves the dominant group for a given satellite image pixel (4 km for the Mediterranean Sea) by identifying which phytoplankton group is the major contributor to the radiance anomaly. In other words, it associates a given phytoplankton type with its main bio-optical signature, while taking into account biases induced by other optically-active components, such as dust deposition events and rivers discharge. From this high-resolution database (about 6,600 daily images), 10-day and monthly maps of dominant phytoplankton groups were obtained by calculating the phytoplankton group that was dominant during the integration period (10-day or monthly, respectively) at each geographical pixel, not including "unidentified" pixels. The regional PHYSAT-Med product was validated by comparing the outputs of the algorithm with more than 5,000 in situ measurements analyzed by high-performance liquid chromatography (HPLC) (Navarro et al., 2014, 2017). This PFT grouping model gathers all the wide range of diatoms within a single PFT, simplifying the complex ecological relationship between different diatom species and other environmental conditions such as temperature.

The current flow field is derived from daily absolute geostrophic surface velocities at 1/8° of spatial resolution derived from a Ssalto/Duacs multimission altimeter regional product released in 2016 specific for the

Mediterranean Sea. This product is currently distributed by the Copernicus Marine Environment Monitoring Service (CMEMS).

4. Results

4.1. Dynamical Co-Coherence of Oceanic Flow Features

We first discuss how the flow characterization inferred from a given kinematic quantity differs when evaluated through either Eulerian or Lagrangian functions. The latter are not directly related to instantaneous measurements of such functions, unless some kind of dynamic equilibrium or ergodicity-type property is established. In this case, the time-integrated effect can be effectively related to the instantaneous or averaged spatial patterns (for instance, if the spatial arrangement of eddies at a given time provides information about the typical time evolution of a water parcel). Using daily gridded geostrophic velocities derived from altimetry we compare daily snapshots of the Eulerian vorticity and EKE, denoted by Ω_0 and K_0, respectively (Figures 1a and 1c), and their Lagrangian counterpart evaluated for $T = 40$ days, Ω_{40} and K_{40} (Figures 1b and 1d). Spatial patterns of Ω_T and K_T differ significantly from their Eulerian equivalence whenever the integration time is greater than 15 days (see Figure S1 in Supporting Information S1). Filamentary structures of intense accumulated vorticity and EKE around and within the eddies that could originate from eddy-flow or eddy-eddy interactions are unveiled by the Lagrangian diagnostic but not by the Eulerian one. Furthermore, some structures with high values of vorticity and EKE identified by Ω_0 and K_0 vanish in Ω_{40} and K_{40}, suggesting that these structures are not dynamically persistent, while only the highly coherent flow structures remain as T increases (Figure S2 in Supporting Information S1). The above analysis suggests that the Lagrangian characterization of the marine turbulent flow unveils supercoherent structures, that is, singular structures of high dynamical coherence (high LCR values), that cannot be identified in the classical Eulerian framework.

To assess how the Ω_T and K_T scale with the duration of integration, we analyze their statistical behavior comparing the probability density functions (PDF) of Ω_T and K_T for different T values for the whole Mediterranean Sea (Figures 1e and 1f). As T increases the peak of the PDFs increases while their width narrows, and the PDFs become more and more asymmetrical, with a pronounced tail for negative vorticity values and high EKE values. This behavior—that of a time-dependent histograms whose peak becomes sharper as the time integration lengthens—is characteristic of multifractal scaling (Falconer, 1990; Hernández-Carrasco et al., 2011), often used to interpret spatial scales but extended here to temporal scales.

Given that in the ocean nearly 80% of the total kinetic energy is captured in vortical coherent structures (Klein et al., 2019), a relationship between Eulerian EKE and vorticity may be expected. However when comparing the spatial patterns of both Eulerian quantities (Figures 1a and 1c), we do not find a clear correspondence. Conversely, the spatial distribution of the filamentary structures obtained from their Lagrangian counterparts, although with peaks that do not perfectly coincide, are very similar (Figures 1b and 1d). To further study the relationship between Ω_T and K_T we examine the histograms of Ω_T conditioned by the value of K_T for different values of T (Figure 2). It allows exploring which aspects of the flow dynamical coherence is well-captured by the Lagrangian assessment but missed by the Eulerian approach. We observe a dispersed cloud of points for $T = 0$ days (Figure 2a), while a modal line (e.g., line of maximum conditioned probabilities) formed by two different, nearly straight, segments is clearly evident for $T = 40$ days (Figure 2b). These segments are associated with a slowly increasing and faster decreasing dependency of Ω_T with K_T, respectively. In order to verify if a functional dependence between vorticity and EKE could hold for our data set, we compute various conditioned averages $\hat{\Omega}_T(K_T)$ for different integration times T (Figure 2c). The plot shows conditioned averages, but the conditioned standard deviation is not negligible as reflected by the correlation coefficients R^2 and associated slopes reported in the caption of Figure 2. While there is a very weak relationship among Eulerian quantities (black curve), we observe more robust relationships as T increases (green curves). The resulting conditional mean is a constant value for K_T smaller than 0.13 m^2/s^2 suggesting that Ω_T and K_T are statistically independent, and there is not a functional relationship between the two variables at low values of EKE. A functional relationship, on the other hand, exists for values of K_T greater than 0.13 m^2/s^2. Overall, Figure 2c suggests that we can approximate Ω_T in terms of $(K_T)^{1/2}$ allowing to infer a spatial scale, L, from the slopes A after fitting: $\Omega_T = A \cdot (K_T)^{1/2}$ $(L = 1/A)$ for high values of $(K_T)^{1/2}$. L has units of length (m) and provides an estimation of the spatial scale associated with the coherence of these Lagrangian structures and their evolution as a function of the time integration. It could be interpreted as the typical length-scales of the vortical structures that contribute most, and for longer

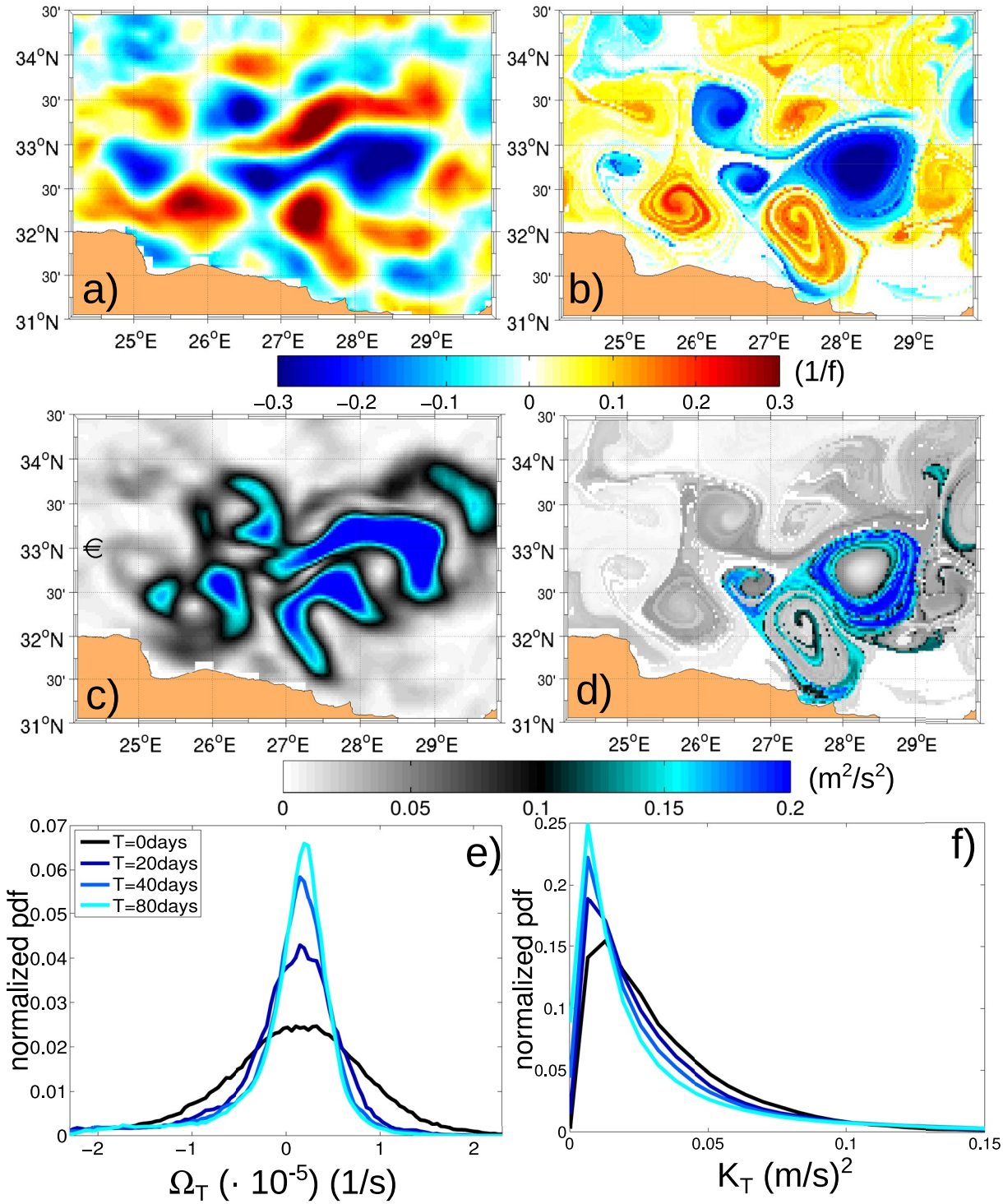

Figure 1. Panels (a) and (b) show snapshots corresponding to 22 March 2016 of Ω_0 and Ω_{40} divided by Coriolis parameter. Panels (c) and (d) show K_0 and K_{40} for the same date. Panels (e) and (f) show the normalized PDF for Ω_T and K_T, respectively, using values from weekly snapshots over 2006–2016 for different integration times, T.

times, to the turbulent energy. Values of L decreases as T increases, with values ranging between [60–15 km] for T = [0–80 days], indicating that when T increases smaller structures are captured. The minimum L value in the flow considered converges to 15 km, which represents the smallest length-scale of the Lagrangian dynamical structures that can be inferred from this velocity field.

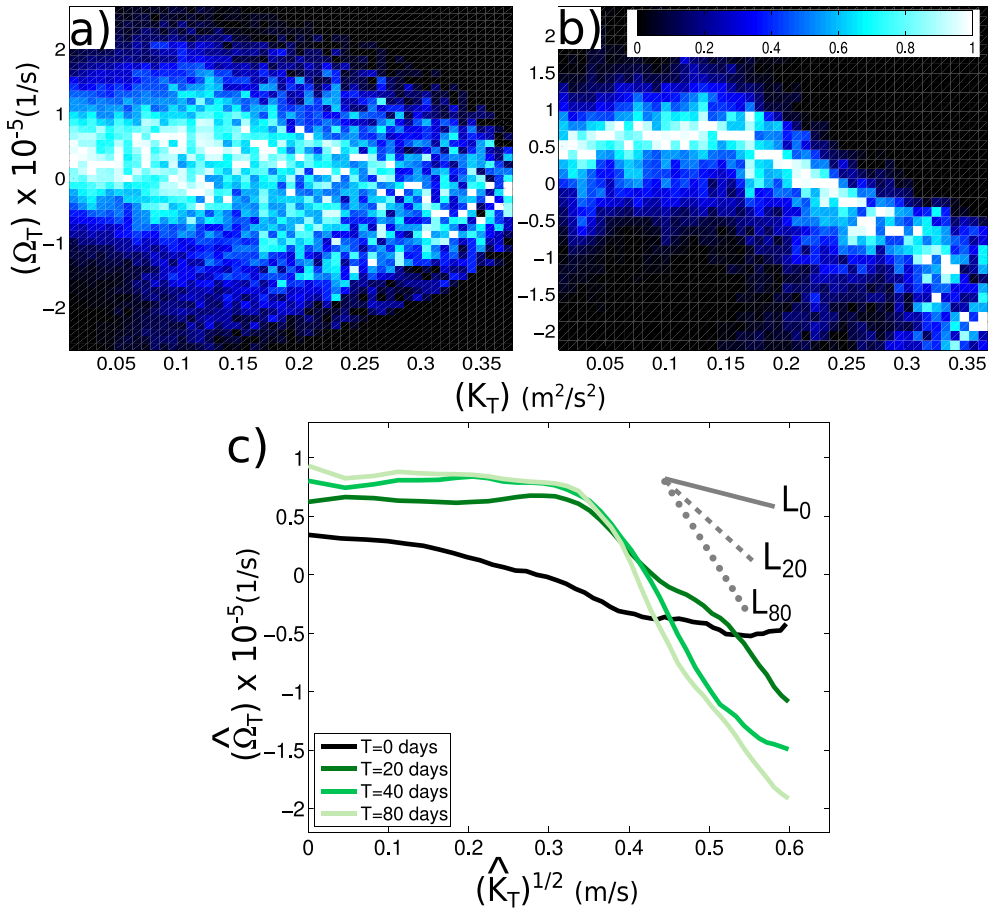

Figure 2. Probability distributions of Ω_T conditioned by K_T for two different time periods of integration, $T = 0$ days (panel a) and $T = 40$ days (panel b). The brightest color (light blue) corresponds to the maximum probability at each column; the darkest color (pure black) corresponds to zero. Panel (c) shows functional dependence between Ω_T versus $K_T^{1/2}$ for different integration times T. Correlation coefficient are computed from co-variance dependence, obtaining $R^2 = 0.19$ for $T = 0$ days; $R^2 = 0.52$ for $T = 20$; $R^2 = 0.69$ for $T = 40$ and $R^2 = 0.76$ for $T = 80$ days. Slopes resulting from the linear regression fit analysis of the functional dependencies between Ω_T versus $K_T^{1/2}$ for $T = 0$, 20 and 80 days are shown as gray lines in (c). Their corresponding length scales are $L_0 = 56$ km, $L_{20} = 29$ km, and $L_{80} = 15$ km.

The high correlation between Ω_T and K_T for $T > 40$ days, indicates that spatial variations of Lagrangian coherent vorticity are closely related to spatial variations of Lagrangian coherent mesoscale activity. This suggests that fluid parcels originated from the persistent anticyclonic eddies analyzed in the Mediterranean Sea area accumulate high mesoscale turbulent energy. Consequently, Ω_T for $T > 40$ days is a more suitable Lagrangian diagnostic to link turbulence properties to phytoplankton dynamics than its Eulerian counterpart ($T = 0$ days), whenever the analyzed flow is derived from altimetry at the currently available resolution.

4.2. Influence of Oceanic Coherence on the Phytoplankton Community Composition

Here we dive on the response of diatoms to the ocean physical conditions focusing on the LCR of the marine flow structures unveiled by this novel methodological approach. Figure 3a shows a patchy spatial distribution of chlorophyll-a concentration, a proxy of total phytoplankton, with local maxima dominated by diatoms (Figure 3b), located at 38.5°N/5.5°E. In order to compare with PHYSAT-Med images, which correspond to the distribution of phytoplankton types retrieved from 10 days-averaged images of ocean color, we show the spatial patterns of time averaged snapshots of Eulerian vorticity, Ω_0, and EKE, K_0, over the same 10 days in Figures 3c and 3e. The two subplots reveal different structures of high vorticity and EKE distributed throughout the entire area. These maps are significantly different from their Lagrangian counterparts Ω_{40} (Figure 3d) and K_{40} (Figure 3f) for $T = 40$ days. Note that T is a Lagrangian time scale (namely LCR) associated with the material

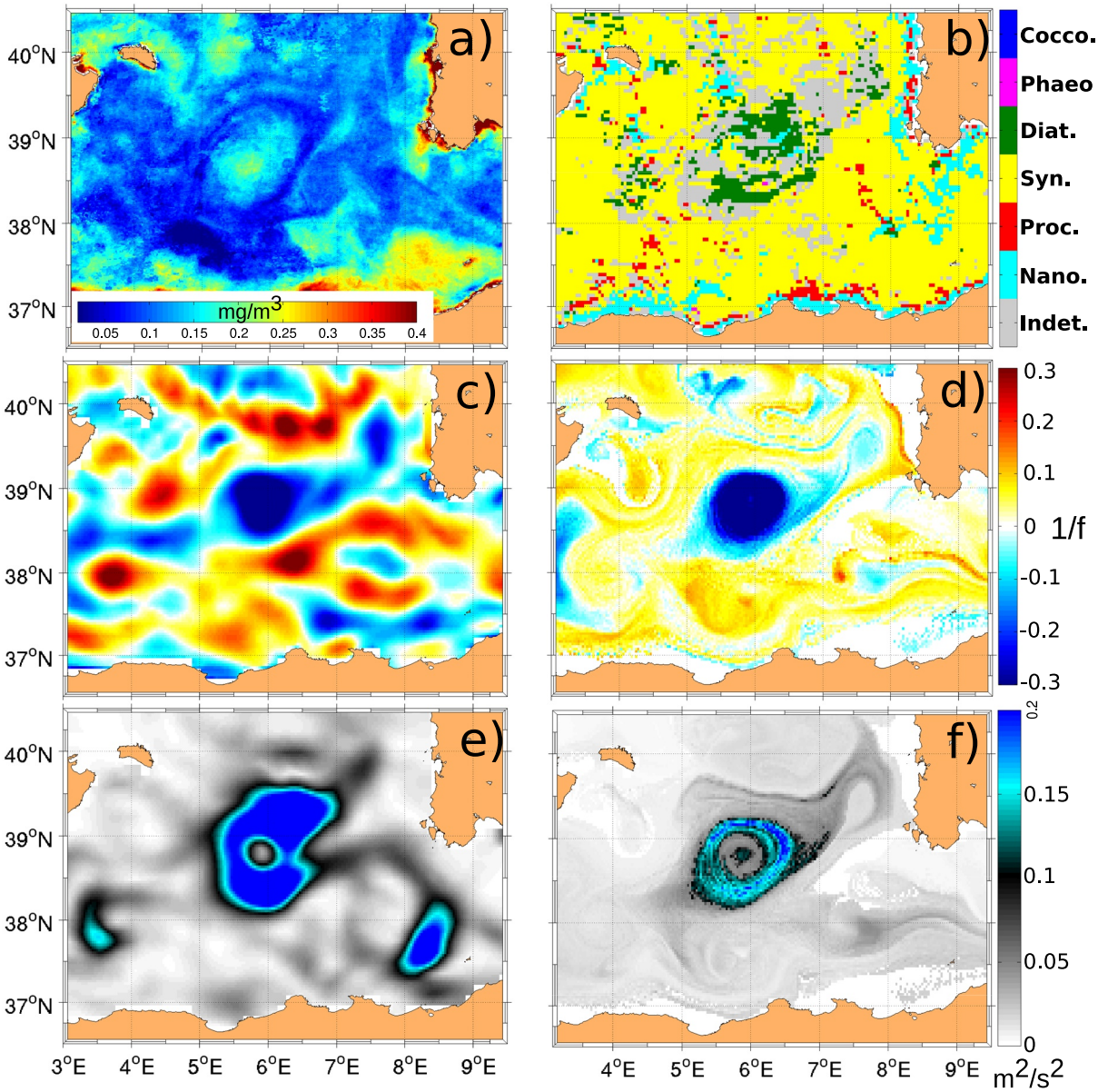

Figure 3. Panel (a) shows a Chlorophyll (*a*) (in mg/m^3) derived from Ocean color; Panel (b) map of dominant phytoplankton functional types retrieved from the PHYSAT-Med product corresponding to the period: 28 May 2009–07 June 2009; Panels (c) and (e) are the Eulerian vorticity, Ω_0, divided by Coriolis, and Eulerian EKE, K_0 (in m^2/s^2), both averaged over 10 daily snapshots (28 May 2009–07 June 2009); Panels (d) and (f) are the Lagrangian vorticity, Ω_{40}, and Lagrangian EKE, K_{40} (in m^2/s^2), for $T = 40$ days, and averaged over the same period.

average, while the time average over 10 days are associated with an Eulerian average (i.e. at the same position). In Ω_{40} and K_{40} only one intense eddy-like structure stands out among all the structures inferred from Ω_0 and K_0. It indicates again that while Eulerian flow structures assess coherence in the spatial domain, Lagrangian structures can assess material coherence in space and time simultaneously. As such, most-eddy like structures identified by Ω_0 and K_0 and vanishing in the Ω_T and K_T fields for $T > 40$ days exhibit spatial coherence only; conversely, the central eddy is unique exhibiting high coherence over both space and time. By combining both Lagrangian metrics we can identify singular supercoherent vortical objects associated with high mesoscale turbulent energy which should impact plankton communities.

Comparing the maps of Ω_0 and K_0 (Figures 3c and 3e), respectively with the spatial distribution of the dominant phytoplankton groups (Figure 3b) we observe that the confined and circular patch dominated by diatoms is

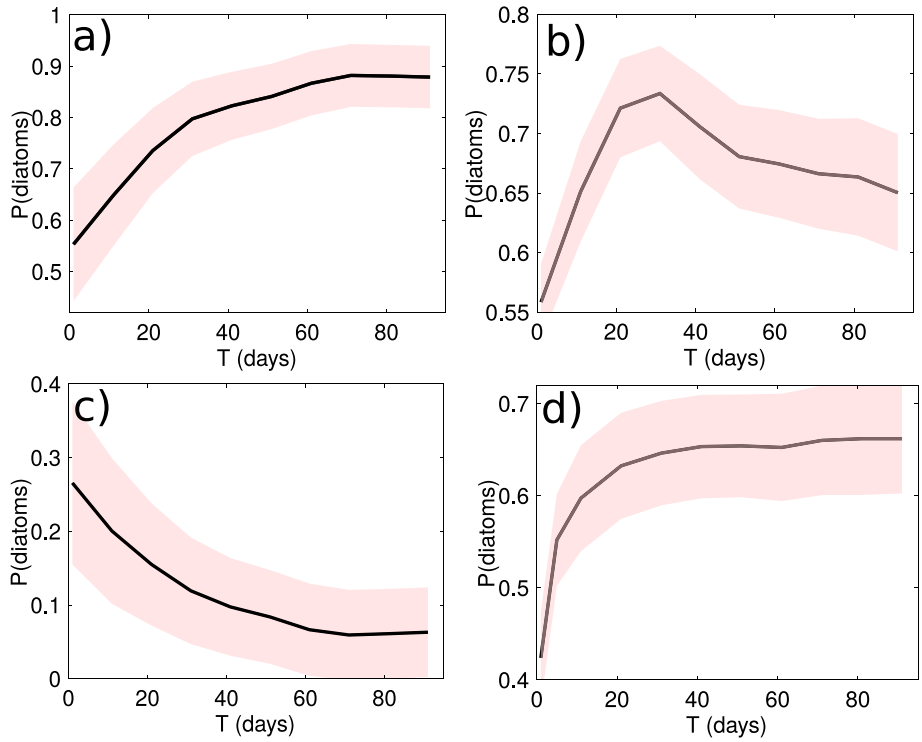

Figure 4. Normalized diatom abundances, P(diatoms), as a function of the time integration T found in regions of high negative Ω_T (panel a); of high positive Ω_T (panel c); of high K_T (panel b); and finally of both high negative Ω_T and high K_T simultaneously (panel d).

associated with local maxima of EKE and extrema (both positive and negative) of vorticity. However, the reciprocal statement is not true: not all local maxima of both Eulerian quantities are characterized by diatoms. Focusing on the Ω_T and K_T diagnostics (Figures 3d and 3f), the singular structure associated with high Lagrangian turbulent kinetic energy and vorticity uniquely identifies the diatoms bloom. In the Eulerian framework, many structures of high EKE and vorticity are present in the domain without a clear correspondence with any dominant phytoplankton group. Conversely, the Lagrangian diagnostics distinguish singular coherent structures that support specific biological response from the other transient features that have no clear biological signal. Further examples of the correspondence between these coherent dynamical objects and diatom blooms are shown in Supporting Information S1 (Figures S3 to S11).

The co-occurrence between diatoms blooms and these singular dynamical structures suggests a relationship between the abundance of diatoms and the degree of coherence of the oceanic features. To further explore this relationship and in order to estimate the optimal LCR that maximizes bio-physical interactions, we compute the normalized number of pixels where diatoms dominate (i.e., the number of pixels identified as diatoms divided by the total number of pixels in the area of high Ω_T and high K_T, henceforth referred to as P(diatoms) which is a proxy of diatoms relative abundance) over regions characterized by high values of Ω_T and K_T fields (defined as $\Omega_T/f > 0.1$ or <-0.1 for negative vorticity and $K_T > 0.1$ m^2/s^2) as a function of T. The abundance of diatoms increases in regions of high negative Ω_T (Figure 4a) while decreases in regions of positive Ω_T as T increases (Figure 4c). This asymmetric behavior is opposite to that recovered through Eulerian analyses (Ω_0) in which diatoms appear associated predominantly with coherent (in space only) positive vorticity. This counter-intuitive behavior is explained by the fact that fluid parcels with positive/negative vorticity at time t_0 may have had opposite sign vorticity when the whole history of the parcel is considered (i.e., integrating the relative vorticity backward in time from t_0 to $t_0 - T > 0$ days). For example, fluid parcels coming from an anticyclonic/cyclonic eddy can be absorbed by an cyclonic/anticyclonic eddy (Hernández-Carrasco et al., 2020). By time-integrating over the flow parcel motions, we are bringing out the overall impact of the submesoscale upwelling associated with mesoscale anticyclonic structures, which has been shown, from both modeling and observational studies, to be persistent (Zhong et al., 2017) and to have a large impact on the primary production (Brannigan, 2016; Hong

et al., 2023; Lévy et al., 2012). For both high negative and positive Ω_T we observe a plateau in P(diatoms) for $T > 70$ days. A similar behavior is identified when looking at P(diatoms) in regions of high Lagrangian turbulent kinetic energy ($K_T > 0.1$ m^2/s^2) for different T. The probability to find high abundance of diatoms increases with T and reaches its maximum value for $T = 30$ days (Figure 4b). By simultaneously conditioning the abundance of diatoms in regions of high Ω_T (either positive or negative) together with K_T (Figure 4d), we find that P(diatoms) associated with these mesoscale turbulent flow conditions initially increases over integration time and reaches a plateau for T (LCR) > 40 days. The drifting fluid parcels that largely contribute to promoting diatom growth are those that preserve high negative vorticity and EKE while they move with the flow for a sufficiently long amount of time. From this LCR threshold, one can infer the optimal coherence time of vortical structures for diatoms blooms under stratified, oligotrophic conditions.

5. Discussion and Conclusions

To understand the effects of global warming on global ocean physical and biogeochemical properties, it is essential to identify the scales that are relevant for dynamical and biological interactions, and then predict their evolution. The coherence analysis of the surface ocean dynamics through the LCR computed from the Lagrangian descriptors K_T and Ω_T, provides for the first time a theoretically-grounded and objective measure of the range of dynamical coherence time and spatial scales associated with mesoscale ocean features. We show that the relationship between EKE (K_T) and vorticity (Ω_T) emerges for topological structures characterized with high LCR. As T increases the Lagrangian vorticity and the EKE field emerge organized in filaments of high values. In the case of the altimetry velocity field analyzed here, we find a dynamical resolution barrier with Lagrangian flow structures size converging and collapsing at spatial scale $L = [15–20$ km] for time scales of coherence $T > 40$ days. At these scales the filamentary dynamics associated with the fine-mesoscale turbulence becomes relevant. This is likely due to the vortex filaments induced by the (mesoscale) eddy-eddy interactions and their contribution to the energy cascade from large to small scales (in nature down to the submesoscales, which are not well captured by current altimetry, but will be partially resolved by the future SWOT mission (Morrow et al., 2019)). This Lagrangian similarity between different kinematic flow properties can be used to assess the finest effective scales of the Lagrangian dynamics captured in a given velocity field. Although the generality of the methodological approach should be investigated in other oceanic regions using global products. In this work, we present the method, its potential and its application to the Mediterranean basin as a case study.

The Lagrangian description of vorticity and eddy kinetic energy through Ω_T and K_T does offer advantages over the conventional Eulerian description. The Lagrangian objects uniquely identified as high-coherent mesoscale eddies track the favorable dynamical conditions, namely a hydrodynamic environment that is materially (in the Lagrangian sense) coherent in space and for a sufficiently long time, favoring diatoms growth. This allows to differentiate the mesoscale structures that effectively promote diatoms blooms from those that only stir existing communities (d'Ovidio et al., 2010). Analyzing the accumulated effect of the flow dynamical properties along fluid parcel trajectories hosting phytoplankton cells allows for estimating the typical time and length scales at which the interactions between the dynamical flow and the fast-growing opportunist planktonic groups (diatom-like in our case) are most significant. We observe that LCR = 40 days is a critical coherence time scale at which the mesoscale turbulent conditions (i.e., vorticity and EKE) influence phytoplankton community composition by promoting diatoms, by favoring both persistent cell re-suspension and nutrient vertical fluxes in the euphotic zone.

The time scale of 40 days found for the Mediterranean Sea is of the same order of magnitude but slightly smaller than the 60 days of mean life associated with non-linear eddies that display the maximum correlation with high concentrations of surface Chl *a* reported in previous studies (Chelton et al., 2011). Other works also showed a time scale of 86 days associated with a sustained diatom bloom observed in the Southern Ocean based on in-situ Si isotopic measurements (Closset et al., 2014). We cannot exclude that different time scales may be found in other ocean basins. The scale may depend on the physical characteristics of the mesoscale structures governing the flow in the area considered or in the biological response given local light and temperature. The methodology presented in this paper is, however, general and can be extended to any other region.

Although the objective of the study is to provide evidence of the dynamical coherence scales of the flow associated with the growth of diatoms, the satellite-derived geostrophic velocity fields do not allow a detailed investigation of the small scale processes that delineate coherent upwelling/downwelling or convergence/divergence, which

have been shown to be important by previous studies (Hernández-Carrasco et al., 2018; Huntley et al., 2015). The limited resolution of the altimetry currents implies that we cannot quantify the biological response to submesoscale dynamics. It should be noted that using a coarse velocity field (coarser than in the real ocean) may introduce spurious Lagrangian dynamics at small scales (Haza et al., 2016), but does not impact the dynamics at scales larger than resolution, which remains robust (Beron-Vera et al., 2019; Hernández-Carrasco et al., 2011). This ensures that the resolution in the altimetry dynamical fields is not affecting the evaluation of the temporal scales at or above 40 days at which diatoms 'feel' the flow coherence. This is evident in Figure 4c, where the concentration of diatoms in structures of high vorticity increases as a function of Lagrangian integration up to $T = 70$ days, which is longer than the critical scale of 40 days identified by the Lagrangian effective resolution analysis. Although a further generalization to other systems should be performed, our findings, based on satellite observations, provide a robust target against which models developed for the Mediterranean Sea can be now tested to verify their ability to properly represent physical-biogeochemical interactions. Mesoscale resolving regional simulations should indeed capture the diatom preferences, at the relevant spatial and temporal coherence scales, that we identified in the satellite observations.

Finally, we stress that in interpreting our results, we excluded the possibility that the fluid parcels with high diatom concentrations are composed of nutrient rich coastal waters by analyzing the origin maps shown in Supporting Information S1 (Figures S12–S14). This suggests that diatom growth occurs in the open ocean whenever resting diatoms spores, likely present in most of the surface ocean (Rynearson et al., 2013) (even oligotrophic), are entrained in coherent physical structures and can exploit vertical mixing events (e.g., ephemeral hot spots of intense vertical fluxes (D. McGillicuddy et al., 1998; Falkowski et al., 1998; Klein & Lapeyre, 2009; Lévy et al., 2018)) induced by specific mesoscale eddies that persist for enough time (in the Mediterranean Sea for more than 1 month). Indeed, our analysis allows for identifying these short-living and moving diatoms habitats despite high-stratification conditions typical of "oceanic deserts," as the major oligotrophic gyres of the world ocean.

Data Availability Statement

Absolute geostrophic velocity data are available on the CMEMS web platform https://data.marine.copernicus.eu/products, https://doi.org/10.48670/moi-00141. PHYSAT-Med data are referenced at Navarro et al., 2017 and are available at https://nimbus.imedea.uib-csic.es/index.php/s/6w6YzWBpTmWD8BW. The code to compute the particle trajectories and the Finite-Time Lagrangian diagnostics are available at https://zenodo.org/record/7705122, https://doi.org/10.5281/zenodo.7705122 (Hernandez-Carrasco, 2023) with Creative Commons Attribution 4.0 International licence. Figures are plotted using Matlab v2021 software available under licence at https://es.mathworks.com/academia/tah-portal/uib-31521075.html.

Acknowledgments
IH-C acknowledges financial support from the project TRITOP (Grant UIB2021-PD06) funded by University of the Balearic Islands and by FEDER(EU). AO thanks financial support from Projects LAMARCA (PID2021-123352OB-C31) funded by MICIN/AEI/10.13039/501100011033/FEDER, UE and Tech2Coast (TED2021-130949B-I00) funded by MCIN/AEI/10.13039/501100011033 and BY EU 'NextGenerationEU/PRTR'. This work has been partially done in the framework of the AEI accreditation "Maria de Maeztu Centre of Excellence" given to IMEDEA (CSIC-UIB) (CEX2021-001198). AB acknowledges support from the National Science Foundation (Grant OCE-1658174). This study is based upon work from the CSIC Interdisciplinary Thematic Platform Teledeteccion (PTI-TELEDETECT) members.

References

Alvain, S., Moulin, C., Dandonneau, Y., & Bréon, F. (2005). Remote sensing of phytoplankton groups in case 1 waters from global SeaWiFS imagery. *Deep Sea Research Part I: Oceanographic Research Papers*, *52*(11), 1989–2004. https://doi.org/10.1016/j.dsr.2005.06.015

Barton, A. D., Dutkiewicz, S., Flierl, G., Bragg, J., & Follows, M. J. (2010). Patterns of diversity in marine phytoplankton. *Science*, *327*(5972), 1509–1511. https://doi.org/10.1126/science.1184961

Barton, A. D., Irwin, A. J., Finkel, Z. V., & Stock, C. A. (2016). Anthropogenic climate change drives shift and shuffle in North Atlantic phytoplankton communities. *Proceedings of the National Academy of Sciences*, *113*(11), 2964–2969. https://doi.org/10.1073/pnas.1519080113

Basterretxea, G., Font-Muñoz, J. S., Salgado-Hernanz, P., Arrieta, J., & Hernández-Carrasco, I. (2018). Patterns of chlorophyll interannual variability in Mediterranean biogeographical regions. *Remote Sensing of Environment*, *215*, 7–17. https://doi.org/10.1016/j.rse.2018.05.027

Beron-Vera, F. J., Hadjighasem, A., Xia, Q., Olascoaga, M. J., & Haller, G. (2019). Coherent Lagrangian swirls among submesoscale motions. *Proceedings of the National Academy of Sciences of the United States of America*, *116*(37), 18251–18256. https://doi.org/10.1073/pnas.1701392115

Brannigan, L. (2016). Intense submesoscale upwelling in anticyclonic eddies. *Geophysical Research Letters*, *43*(7), 3360–3369. https://doi.org/10.1002/2016GL067926

Chelton, D., Gaube, P., Schlax, M., Early, J., & Samelson, R. (2011). The influence of nonlinear mesoscale eddies on near-surface oceanic chlorophyll. *Science*, *334*(6054), 328–332. https://doi.org/10.1126/science.1208897

Closset, I., Lasbleiz, M., Leblanc, K., Quéguiner, B., Cavagna, A.-J., Elskens, M., et al. (2014). Seasonal evolution of net and regenerated silica production around a natural Fe-fertilized area in the Southern Ocean estimated with Si isotopic approaches. *Biogeosciences*, *11*(20), 5827–5846. https://doi.org/10.5194/bg-11-5827-2014

Cotti-Rausch, B. E., Lomas, M. W., Lachenmyer, E. M., Goldman, E. A., Bell, D. W., Goldberg, S. R., & Richardson, T. L. (2016). Mesoscale and sub-mesoscale variability in phytoplankton community composition in the Sargasso Sea. *Deep Sea Research Part I: Oceanographic Research Papers*, *110*, 106–122. https://doi.org/10.1016/j.dsr.2015.11.008

d'Ovidio, F., Isern-Fontanet, J., López, C., Hernández-García, E., & García-Ladona, E. (2009). Comparison between Eulerian diagnostics and finite-size Lyapunov exponents computed from altimetry in the Algerian basin. *Deep-Sea Research I*, *56*(1), 15–31. https://doi.org/10.1016/j.dsr.2008.07.014

d'Ovidio, F., Monte, S., Alvain, S., Dandonneau, Y., & Levy, M. (2010). Fluid dynamical niches of phytoplankton types. *Proceedings of the National Academy of Sciences of the United States of America*, *107*(43), 18366–18370. https://doi.org/10.1073/pnas.1004620107

Falconer, K. (1990). *Fractal geometry: Mathematical foundations and applications*. John Wiley and sons.

Falkowski, P. G., Barber, R. T., & Smetacek, V. (1998). Biogeochemical controls and feedbacks on ocean primary production. *Science*, *281*(5374), 200–206. https://doi.org/10.1126/science.281.5374.200

Field, C. B., Behrenfeld, M. J., Randerson, J. T., & Falkowski, P. (1998). Primary production of the biosphere: Integrating terrestrial and oceanic components. *Science*, *281*(5374), 237–240. https://doi.org/10.1126/science.281.5374.237

Frémont, P., Gehlen, M., Vrac, M., Leconte, J., Delmont, T. O., Wincker, P., et al. (2022). Restructuring of plankton genomic biogeography in the surface ocean under climate change. *Nature Climate Change*, *12*(4), 393–401. https://doi.org/10.1038/s41558-022-01314-8

Gaube, P., McGillicuddy, D. J., Jr., & Moulin, A. J. (2019). Mesoscale eddies modulate mixed layer depth globally. *Geophysical Research Letters*, *46*(3), 1505–1512. https://doi.org/10.1029/2018GL080006

Haller, G. (2016). Dynamic rotation and stretch tensors from a dynamic polar decomposition. *Journal of the Mechanics and Physics of Solids*, *86*, 70–93. https://doi.org/10.1016/j.jmps.2015.10.002

Haller, G., Hadjighasem, A., Farazmand, M., & Huhn, F. (2016). Defining coherent vortices objectively from the vorticity. *Journal of Fluid Mechanics*, *795*, 1136–1173. https://doi.org/10.1017/jfm.2016.151

Haller, G., & Poje, A. (1998). Finite time transport in aperiodic flows. *Physica D*, *119*(3–4), 352–380. https://doi.org/10.1016/s0167-2789(98)00091-8

Haza, A., Özgökmen, T., & Hogan, P. (2016). Impact of submesoscales on surface material distribution in a Gulf of Mexico mesoscale eddy. *Ocean Modelling*, *107*, 28–47. https://doi.org/10.1016/j.ocemod.2016.10.002

Hernandez-Carrasco, I. (2023). Lagrangian integration of 2D flow kinematics properties. Zenodo. https://doi.org/10.5281/ZENODO.7705122

Hernández-Carrasco, I., Alou-Font, E., Dumont, P.-A., Cabornero, A., Allen, J., & Orfila, A. (2020). Lagrangian flow effects on phytoplankton abundance and composition along filament-like structures. *Progress in Oceanography*, *189*, 102469. https://doi.org/10.1016/j.pocean.2020.102469

Hernández-Carrasco, I., López, C., Hernández-García, E., & Turiel, A. (2011). How reliable are finite-size Lyapunov exponents for the assessment of ocean dynamics? *Ocean Modelling*, *36*(3–4), 208–218. https://doi.org/10.1016/j.ocemod.2010.12.006

Hernández-Carrasco, I., Orfila, A., Rossi, V., & Garçon, V. (2018). Effect of small-scale transport processes on phytoplankton distribution in coastal seas. *Scientific Reports*, *8*(1), 8613. https://doi.org/10.1038/s41598-018-26857-9

Hong, T. T. M., Park, Y.-G., & Choi, J. M. (2023). Divergence observation in a mesoscale eddy during chl *a* bloom revealed in submesoscale satellite currents. *Remote Sensing*, *15*(4), 995. https://doi.org/10.3390/rs15040995

Huntley, H. S., Lipphardt, B. L., Jacobs, G., & Kirwan, A. D. (2015). Clusters, deformation, and dilation: Diagnostics for material accumulation regions. *Journal of Geophysical Research: Oceans*, *120*(10), 6622–6636. https://doi.org/10.1002/2015JC011036

Klein, P., & Lapeyre, G. (2009). The oceanic vertical pump induced by mesoscale and submesoscale turbulence. *Annual Review of Marine Science*, *1*, 351–375. https://doi.org/10.1146/annurev.marine.010908.163704

Klein, P., Lapeyre, G., Siegelman, L., Qiu, B., Fu, L.-L., Torres, H., et al. (2019). Ocean-scale interactions from space. *Earth and Space Science*, *6*(5), 795–817. https://doi.org/10.1029/2018EA000492

Lévy, M., Ferrari, R., Franks, P., Martin, A. P., & Riviere, P. (2012). Bringing physics to life at the submesoscale. *Geophysical Research Letters*, *39*(14), L14602. https://doi.org/10.1029/2012GL052756

Lévy, M., Franks, P., & Smith, K. (2018). The role of submesoscale currents in structuring marine ecosystems. *Nature Communications*, *9*(1), 4758. https://doi.org/10.1038/s41467-018-07059-3

Lévy, M., Jahn, O., Dutkiewicz, S., & Follows, M. J. (2014). Phytoplankton diversity and community structure affected by oceanic dispersal and mesoscale turbulence. *Limnology and Oceanography: Fluids and Environments*, *4*(1), 67–84. https://doi.org/10.1215/21573689-2768549

Liu, G., Bracco, A., & Sitar, A. (2021). Submesoscale mixing across the mixed layer in the Gulf of Mexico. *Frontiers in Marine Science*, *8*. https://doi.org/10.3389/fmars.2021.615066

Malviya, S., Scalco, E., Audic, S., Vincent, F., Veluchamy, A., Poulain, J., et al. (2016). Insights into global diatom distribution and diversity in the world's ocean. *Proceedings of the National Academy of Sciences*, *113*(11), E1516–E1525. https://doi.org/10.1073/pnas.1509523113

McGillicuddy, D., Robinson, A., Siegel, D., Jannasch, H., Johnson, R., Dickey, T., et al. (1998). Influence of mesoscale eddies on new production in the Sargasso Sea. *Nature*, *394*(6690), 263–265. https://doi.org/10.1038/28367

McGillicuddy, D. J. (2016). Mechanisms of physical-biological-biogeochemical interaction at the oceanic mesoscale. *Annual Review of Marine Science*, *8*(1), 125–159. https://doi.org/10.1146/annurev-marine-010814-015606

Mezić, I., Loire, S., Fonoberov, V. A., & Hogan, P. (2010). A new mixing diagnostic and gulf oil spill movement. *Science*, *330*(6003), 486–489. https://doi.org/10.1126/science.1194607

Morales-Márquez, V., Hernández-Carrasco, I., Fox-Kemper, B., & Orfila, A. (2023). Ageostrophic contribution by the wind and waves induced flow to the lateral stirring in the Mediterranean Sea. *Journal of Geophysical Research: Oceans*, *18*(4), e2022JC019135. https://doi.org/10.1029/2022JC019135

Morrow, R., Fu, L.-L., Ardhuin, F., Benkiran, M., Chapron, B., Cosme, E., et al. (2019). Global observations of fine-scale ocean surface topography with the surface water and ocean topography (SWOT) Mission. *Frontiers in Marine Science*, *6*. https://doi.org/10.3389/fmars.2019.00232

Navarro, G., Almaraz, P., Caballero, I., Vazquez, A., & Huertas, I. E. (2017). Reproduction of spatio-temporal patterns of major mediterranean phytoplankton groups from remote sensing OC-CCI data. *Frontiers in Marine Science*, *4*, 246. https://doi.org/10.3389/fmars.2017.00246

Navarro, G., Alvain, S., Vantrepotte, V., & Huertas, I. (2014). Identification of dominant phytoplankton functional types in the mediterranean sea based on a regionalized remote sensing approach. *Remote Sensing of Environment*, *152*, 557–575. https://doi.org/10.1016/j.rse.2014.06.029

Rynearson, T., Richardson, K., Lampitt, R., Sieracki, M., Poulton, A., Lyngsgaard, M., & Perry, M. (2013). Major contribution of diatom resting spores to vertical flux in the sub-polar North Atlantic. *Deep Sea Research Part I: Oceanographic Research Papers*, *82*, 60–71. https://doi.org/10.1016/j.dsr.2013.07.013

Storm, T., Boettcher, M., Grant, M., Zuhlke, M., Fomferra, N., Jackson, T., et al. (2013). Product user guide, ocean colour climate change initiative.

Tréguer, P., Bowler, C., Moriceau, B., Dutkiewicz, S., Gehlen, M., Aumont, O., et al. (2018). Influence of diatom diversity on the ocean biological carbon pump. *Nature Geoscience*, *11*(1), 27–37. https://doi.org/10.1038/s41561-017-0028-x

Wilkins, D., van Sebille, E., Rintoul, S. R., Lauro, F. M., & Cavicchioli, R. (2013). Advection shapes southern ocean microbial assemblages independent of distance and environment effects. *Nature Communications*, *4*(1), 2457. https://doi.org/10.1038/ncomms3457

Zhong, Y., Bracco, A., Tian, J., Dong, J., Zhao, W., & Zhang, Z. (2017). Observed and simulated submesoscale vertical pump of an anticyclonic eddy in the South China Sea. *Scientific Reports*, *7*(1), 44011. https://doi.org/10.1002/jgrc.20402

10.1029/2023GL103688

Erratum

In the originally published version of this article, Section 4.2 contained errors in the seventh sentence of the first paragraph. $\Omega_1 0$ and $K_4 0$ should read Ω_{40} and K_{40}, respectively. The errors have been corrected, and this may be considered the authoritative version of record.